Supporting Information

An organic-inorganic hybrid polyoxoniobate decorated by Co(III)-amine complex for electrocatalytic urea splitting

Da-Huan Li, Nian Shi, Yong-Jiang Wang, Ping-Wei Cai, Yan-Qiong Sun* and Shou-Tian Zheng*

College of Chemistry, Fuzhou University, Fuzhou, Fujian 350108, China.

*Email: sunyq@fzu.edu.cn; stzheng@fzu.edu.cn

Contents

1. Materials and Methods

Chemicals and materials:

Cobalt acetate [$Co(Ac)_2 \cdot 4H_2O$, ≥99.5.0%], boric acid [H_3BO_3, ≥99.0%], sodium carbonate [Na_2CO_3, ≥99.8%], sodium bicarbonate [$NaHCO_3$, ≥99.5%], acetylene black (AB), methyl alcohol [CH_4O, ≥99.0%], absolute ethyl alcohol [C_2H_6O, ≥99.0%] and urea [CH_4N_2O, ≥99.0%] are all analytical grades purchased from Sinopharm Chemical Reagent Co. Ltd. Ethylenediamine [$C_2H_8N_2$, ≥98.0%], 5 wt% of Nafion solution, and 50 wt% of polyethyleneimine (PEI) solution were purchased from Sigma-Aldrich, which were all used without any extra purification.

Synthesis of Co_2Nb_6:

The synthesis of $K_7H[Nb_6O_{19}] \cdot 13H_2O$ (**Nb_6**) was performed based on the reported literature.[1] 0.2828 g $K_7H[Nb_6O_{19}] \cdot 13H_2O$, 0.1151 g $Co(Ac)_2 \cdot 4H_2O$, and 0.0584 g H_3BO_3 were dissolved in 8 mL of $Na_2CO_3/NaHCO_3$ buffer solution (pH = 10.5). Subsequently, 45 μL of ethylenediamine was added to the solution. The mixture was stirred for 1 h, and then heated at 100 ℃ for 96 h. After being cooled slowly to room temperature, the dark green rhombic crystals **Co_2Nb_6** were obtained by further washing with distilled water and drying completely.

Preparation of Co_2Nb_6&AB:

The mixture of 0.25 g of **Co_2Nb_6**, 0.7 mL of PEI, and 0.5 g of AB was uniformly dispersed in 50 mL of methanol. The mixture was stirred for 6 h, and washed with water to generate the final catalyst **Co_2Nb_6&AB**. For the comparison, CoO&AB, **Co_2Nb_6/AB** without PEI and **Nb_6&AB** without Co atoms were synthesized using the same method.

Characterization:

Field emission scanning electron microscopy (FESEM, Nova NanoSEM 230) was used to examine the samples' morphological and microstructural properties. High-resolution TEM (HRTEM) together with its element mapping was carried out on the TEM (FEI Talos F200S G2) to further understand the microstructure details. X-ray photoelectron spectroscopy was used to analyze the samples' surface composition (XPS, ESCALAB 250). Powder X-ray diffraction (PXRD) patterns were obtained on a Rigaku Ultima IV diffractometer, X'PertPRO with Cu-Kα radiation (λ = 1.54056 Å), and MiniFlex II. Infrared (IR) spectra (KBr particles) were obtained using a Nicolet IS

50 FT-IR spectrometer in the range of 400–4000 cm^{-1}. Single-crystal X-ray diffraction data for **Co_2Nb_6** was collected on the Bruker APEX II CCD diffractometer, using MoKα radiation with λ = 0.71073 Å, under nitrogen atmosphere, and at 175 K. The empirical absorption correction was based on equivalent reflections. The crystal structures were solved by the direct method and refined by the full-matrix least-squares method on $F^{2,}$ according to the SHELX and OLEX. The non-hydrogen atoms except some free O atoms are refined with anisotropic thermal parameters. Crystallographic data for the structures reported have been deposited in the Cambridge Crystallographic Data Centre with CCDC reference numbers 2267557 for the compound. These data can be obtained free of charge from the Cambridge Crystallographic Data Centre at www.ccdc.cam.ac.uk/data request/cif. The selected crystal parameters, data collection, and refinements are summarized in Table S1.

Electrochemical characterization:

Electrochemical measurements were performed in the standard three-electrode system of the Zennium-pro (Germany Zahner Instrument) electrochemical workstation. All the electrochemical tests were carried out at room temperature. Graphite rod and Hg/HgO (saturated 1 M KOH solution) electrodes were employed as the counter electrode (CE) and reference electrode (RE), respectively. A homogeneous aqueous solution of catalyst ink was formed by slowly adding 5 mg of sample and 40 μL of Nafion (5 wt% aqueous solutions) to 1 mL of ethanol and keeping it under sonication conditions for 30 min. The carbon cloth (CC) was first degreased by sonication in acetone solution, and then carefully washed with 0.5 M HCl in an ultrasonic bath for 20 min to remove the surface oxidation layer. A working electrode was made by dropping ink containing catalyst on the CC, the catalyst loading on the CC was about 0.5 mg cm^{-2}. In this work, the catalysis of UOR and OER was performed in 1 M KOH (pH = 13.82, 25 °C) with and without 0.33 M urea. All the potentials mentioned for this work were calibrated against the reversible hydrogen electrode (RHE) according to the equation: $E_{RHE} = E_{Hg/HgO} + 0.098 + 0.0591 \times pH$. In particular, the CV tests were first performed at a scan rate of 50 mV s^{-1} for 500 cycles to attain a stable state. Then, LSV curves of UOR and OER were recorded at a scan rate of 5 mV s^{-1}. The Tafel plots were graphed using the Tafel equation, $\eta = b (\log |j|) + a$, in which b is the Tafel slope, and j is the current density. For evaluating the electrochemically active surface area (ECSA), cyclic voltammetry (CV) was performed between 0.925 and 1.025 V at scan rates from 20 to 120 mV s^{-1}. The C_{dl} values were estimated by plotting $\Delta j = (j_a - j_c)$ at 0.975 V against the scan rates, where j_a and j_c are the anode and cathode current densities, respectively. Turnover Frequency (TOF) values were calculated using the TOF = $j \times A_{geo} / (n \times F \times N_{site})$ equation, where j is the current density at a potential, A_{geo} is the electrode area, n is the number of electrons (6 for UOR), F is the Faraday constant (96485 C/mol), and N_{site} is the total number of metal sites. The EIS measurements were performed with an open-circuit potential using an AC voltage of 5 mV amplitude and a frequency range of 10 kHz to 0.01 Hz. In the end, the electrode stability was tested by the chronopotentiometry response.

2. Additional tables

Table S1 Crystal data and structure refinement parameters for Co_2Nb_6.

Compound	**Co_2Nb_6**
Empirical formula	$Co_4Nb_{12}Na_4O_{87}C_{16}N_{16}H_{166}$
M_r (g mol^{-1})	3418.1
Crystal system	triclinic
Space group	*P*
a (Å)	14.4294(7)
b (Å)	17.1065(8)
c (Å)	20.2305(8)
α (°)	96.820(2)
β (°)	105.385(2)
γ (°)	97.235(2)
V (Å^3)	4715.5(4)
Z	2
F (000)	2856
ρ_{calcd} (g cm^{-3})	2.121
Temperature (K)	175(2)
μ (mm^{-1})	2.21
Refl. Collected	147546
Independent relf	16689
Parameters	1099
GOOF	1.046
R_1 [I >2σ]	R_1[a] = 0.0450, wR_2[b] = 0.1303
R_1 (all data)	R_1[a] = 0.0487, wR_2[b] = 0.1336

[a]$R_1 = \sum||F_o|-|F_c||/\sum|F_o|$, [b]$wR_2 = \{\sum[w(F_o^2-F_c^2)^2]/\sum[w(F_o^2)^2]\}^{1/2}$

Table S2. The bond valence sum calculations of the Nb and Co atoms.

Atoms code	Bond Valence	Valence state
Nb1	5.02844	5
Nb2	5.03478	5
Nb3	5.00460	5
Nb4	4.98679	5
Nb5	5.00075	5
Nb6	5.05271	5
Nb7	4.95857	5
Nb8	4.99939	5
Nb9	5.00131	5
Nb10	5.02053	5
Nb11	4.96600	5
Nb12	5.00898	5
Co1	3.12551	3
Co2	2.86734	3
Co3	2.86429	3
Co4	3.14381	3

Table S3. Co_2Nb_6&AB and recently reported catalysts in alkaline electrolytes for overall urea electrolysis performance.

Catalysts	Electrolyte	Voltage for urea electrolysis at corresponding *j* (V@mA/cm^{-2})	Tafel slope (mV dec^{-1})	Ref.
Co_2Nb_6&AB	**1 M KOH + 0.33 M urea**	**1.378@10**	**58.7**	**This work**
NiCo-WO_x/NF	1 M KOH + 0.33 M urea	1.35@10	28	[2]
NCVS-3	1 M KOH + 0.33 M urea	1.35@10	30.31	[3]
$NiFeCoS_x$@$FeNi_3$	1 M KOH + 0.33 M urea	1.42@10	97	[4]
$Co_2Mo_{0.2}CH$	1 M KOH + 0.33 M urea	1.33@10	32	[5]
Co_3Mo_3N-400/NF	1 M KOH + 0.33 M urea	1.356@100	49.4	[6]
CoNiLDH-3	1 M KOH + 0.33 M urea	1.32@0	16	[7]
NCM/G 811	1 M KOH + 0.33 M urea	1.32@10	41	[8]
$Mo_{0.05}$, Co-NSH	1 M KOH + 0.33 M urea	1.6@147.1	64.4	[9]
NiCoP/CC	1 M KOH + 0.5 M urea	1.30@10	49	[10]
$Co_{0.26}$-$Ni(OH)_2$NPs/CF	1 M KOH + 0.5 M urea	1.27@10	34.1	[11]
a-MoS_2/CoS/$Co_{0.85}$Se HNTs	1 M KOH + 0.5 M urea	1.38@50	73.9	[12]
Ni/Co-3	1 M KOH + 0.33 M urea	1.29@0	51.1	[13]
$Co_2Mo_3O_8$	1 M KOH + 0.5 M urea	1.40@100	51.6	[14]
RhSA-P-Co_3O_4	1 M KOH + 0.5 M urea	1.28@10	24	[15]
$CoWO_4$	1 M KOH + 0.5 M urea	1.37@100	28	[16]
Mo-NiCoP@NiCoP /NiXCoYH_2PO_2	1 M KOH + 0.5 M urea	1.348@10	95.21	[17]
NC-FNCP	1 M KOH + 0.5 M urea	1.37@100	35.79	[18]
$AgCoPO_4$/CFP	1 M KOH + 0.5 M urea	1.43@15	49.1	[19]

CoS_x/Co-MOF	1 M KOH + 0.5 M urea	1.315@10	50	[20]
Co-Z/Se-2	1 M KOH + 0.5 M urea	1.39@50	69.8	[21]
N-Ni1$Co_3Mn_{0.4}O$/NF	1 M KOH + 0.5 M urea	1.399@100	143	[22]
S-Co_2P@Ni_2P	1 M KOH + 0.5 M urea	1.36@100	44.5	[23]
Co_3V@C/Co_2VO_4	1 M KOH + 0.5 M urea	1.31@10	43	[24]
Ni-Co_2VO_4/NF	1 M KOH + 0.5 M urea	1.28@10	46	[25]

Table S4. EIS performance parameters of each catalyst.

Samples	R_s/Ω	**CPE/mF**	R_{ct}/Ω
CC	1.67	7.9	884
AB	1.72	3.59	161
Nb_6O_{19}&AB	1.69	4.51	136
$Co(OH)_2$&AB	1.55	3.88	107
Co_2Nb_6&AB	1.41	4.0	81

2. Additional figures

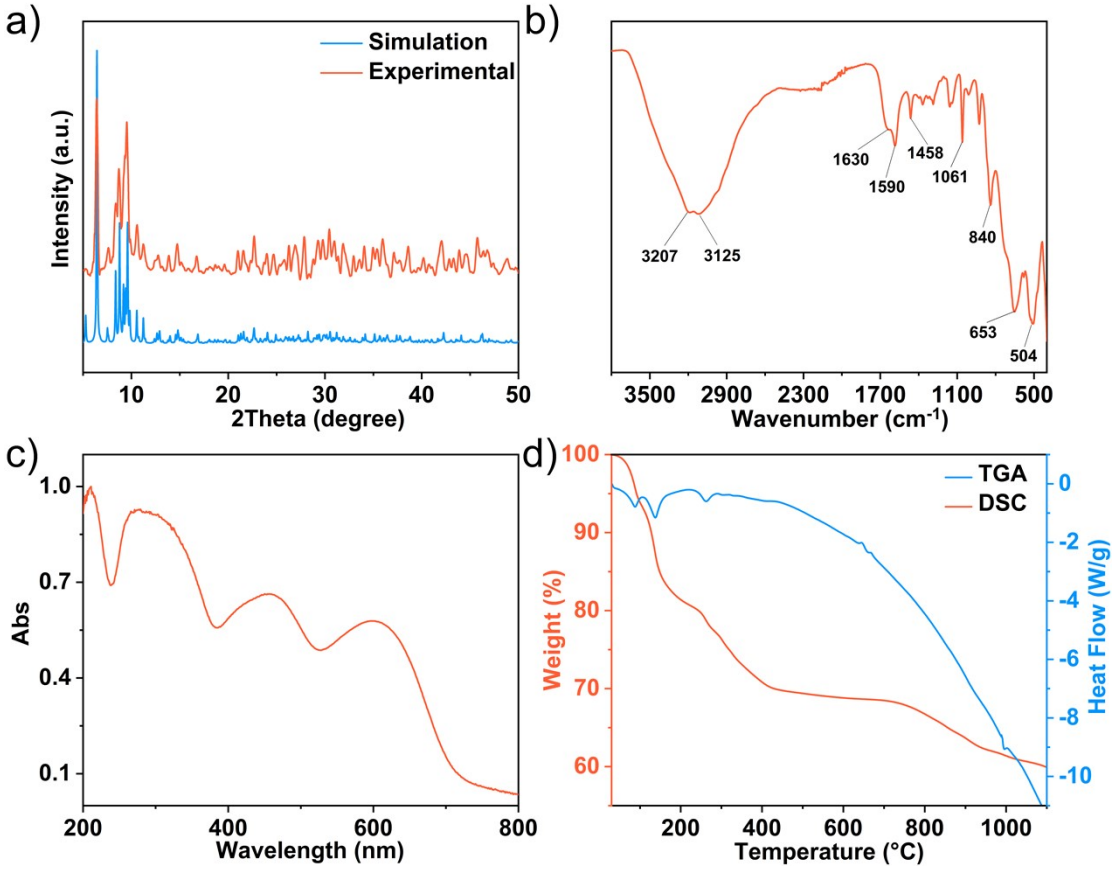

Fig. S1 a) Simulated and experimental PXRD patterns of **Co_2Nb_6**; b) IR spectrum of **Co_2Nb_6**; c) Solid UV diffuse reflection spectrum of **Co_2Nb_6**; d) TGA and DSC curves of **Co_2Nb_6**.

Firstly, the powder X-ray diffraction test was carried out for the sample of **Co_2Nb_6** at room temperature (Fig. S1a†). The peak positions are consistent with the simulated diffraction peak, indicating that the powder sample of the compound powder sample is a pure phase. In addition, the structure of **Co_2Nb_6** was characterized by Fourier transform infrared (FTIR) spectroscopy. As shown in Fig. S1b†, the broad absorption peaks in the range of 3200–3500 cm^{-1} are attributed to the ν (O–H) stretching vibration of water in **Co_2Nb_6**, as well as the matching (H–O–H) bending vibration peaks around 1630 cm^{-1}. The broad absorption peaks in the range of 3000–3200 cm^{-1} are attributed to the ν (C–H) and ν (N–H) stretching vibrations of **Co_2Nb_6**, while the δ (C–H) and δ(N–H) bending vibration peaks are in the range of 1500–1600 cm^{-1}. The peak around 840 cm^{-1} corresponds to the ν (Nb=O_t) absorption peak, while the peaks at 653 cm^{-1} and 504 cm^{-1} belong to the ν (Nb–O_b–Nb). The solid UV diffuse reflectance spectrum of the compound **Co_2Nb_6** is shown in Fig. S1c†, The absorption peaks around 290–450 nm are attributed to the O → Nb charge transfer transition (OMCT), while the absorption peak near 610 nm can be attributed to the d-d transition of the cobalt ion. The thermogravimetric analysis of the compound is shown in Fig. S1d†, from room temperature to 90 °C, the weight loss is 6.12 %, corresponding to 12 free water molecules, with a theoretical value of 6.31 %. When the first plateau was reached (600 °C), the weight loss was 24.92 %, corresponding to the loss of 22 free water molecules, 15 ligand water molecules, and 3 ethylenediamine molecules, with a theoretical value of 24.76 %. At 1000–1100 °C, the weight loss was 8.68 %, corresponding to the loss of all water molecules and 8 ethylenediamine molecules, with a theoretical value of 8.61 %.

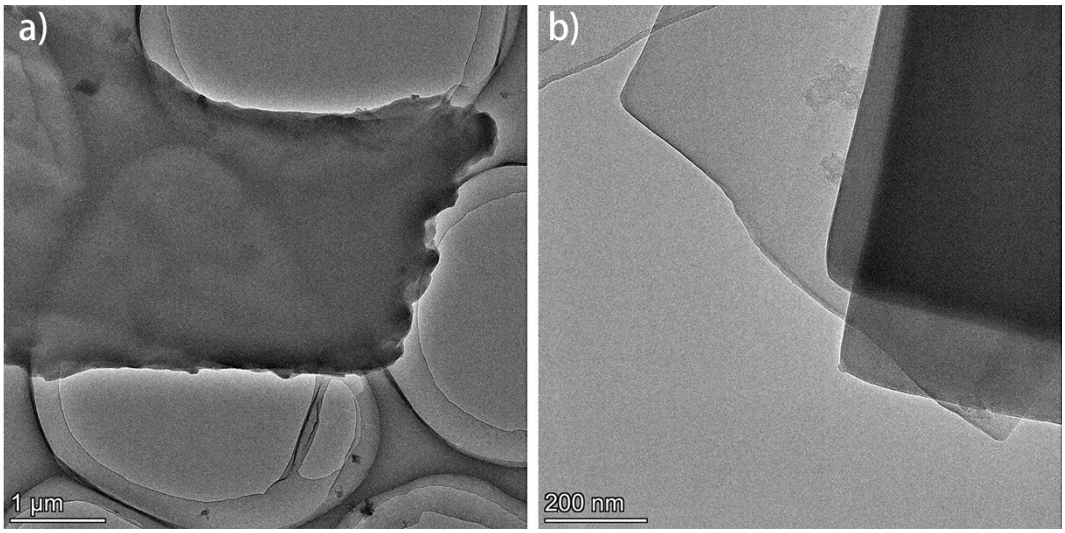

Fig. S2 TEM images of **Co_2Nb_6&AB** with different magnifications.

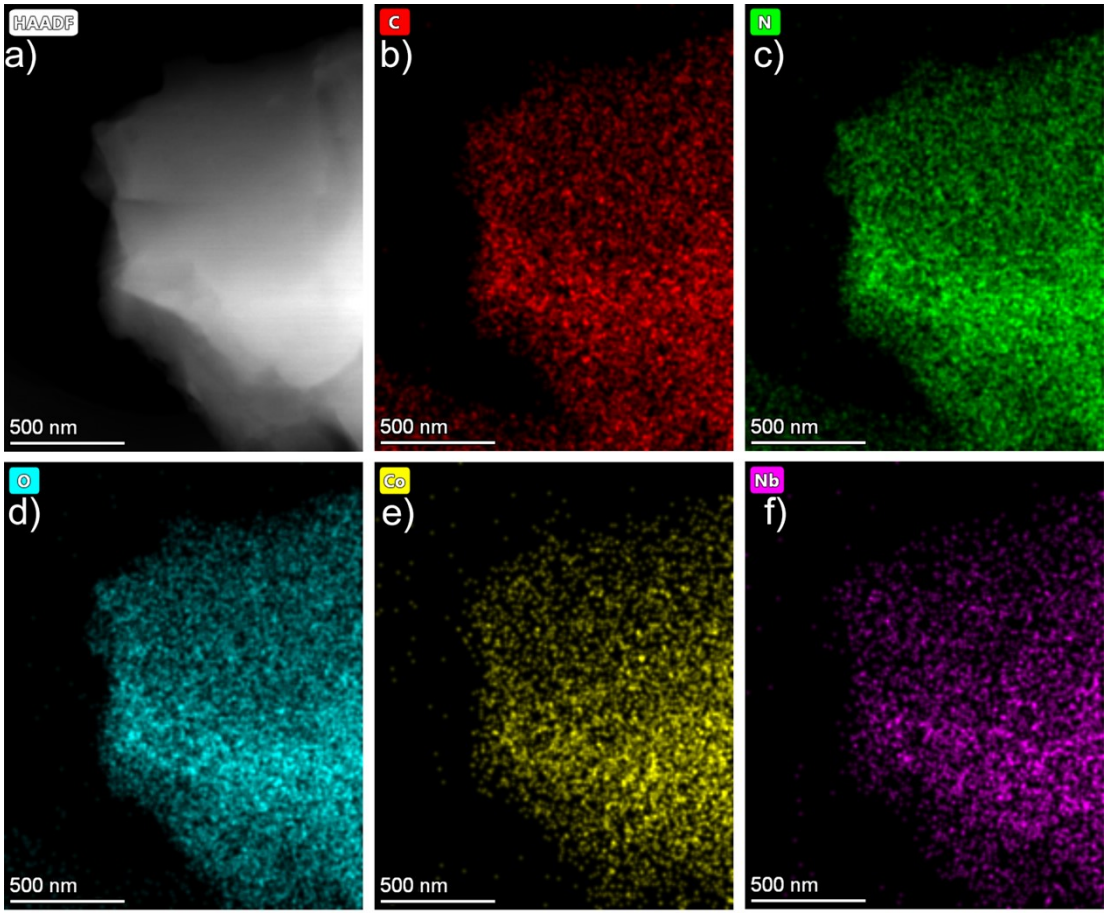

Fig. S3 a) TEM of **Co_2Nb_6&AB** and corresponding elemental distribution mapping images of b) C, c) N, d) O, e) Co and f) Nb.

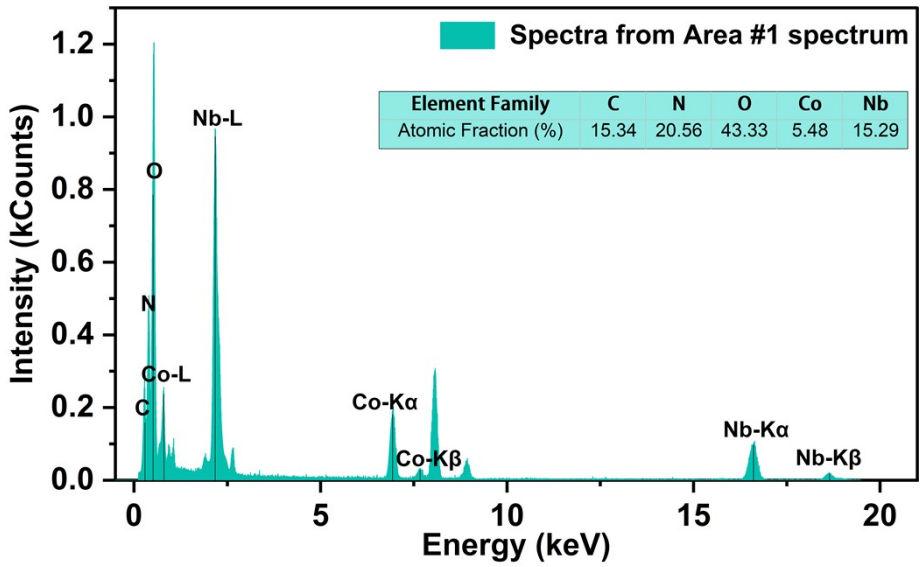

Fig. S4 EDX spectrum of **Co_2Nb_6&AB**.

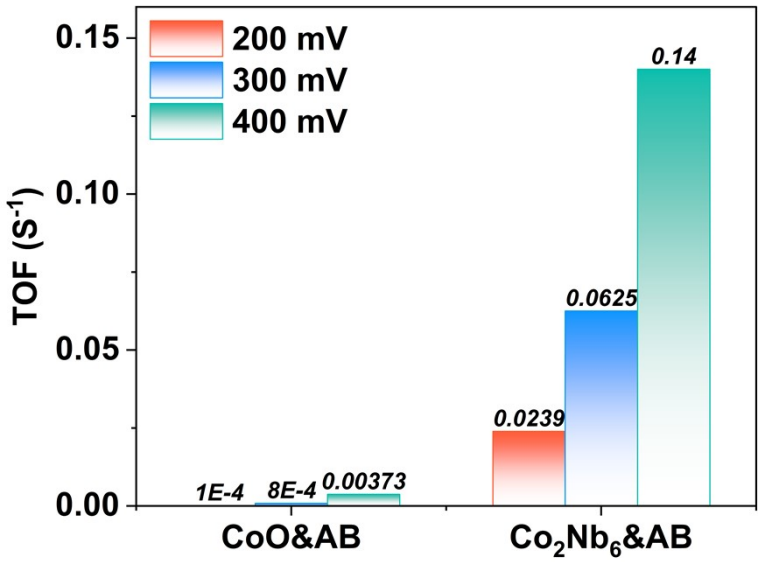

Fig. S5 TOF values of CoO&AB and **Co_2Nb_6&AB**.

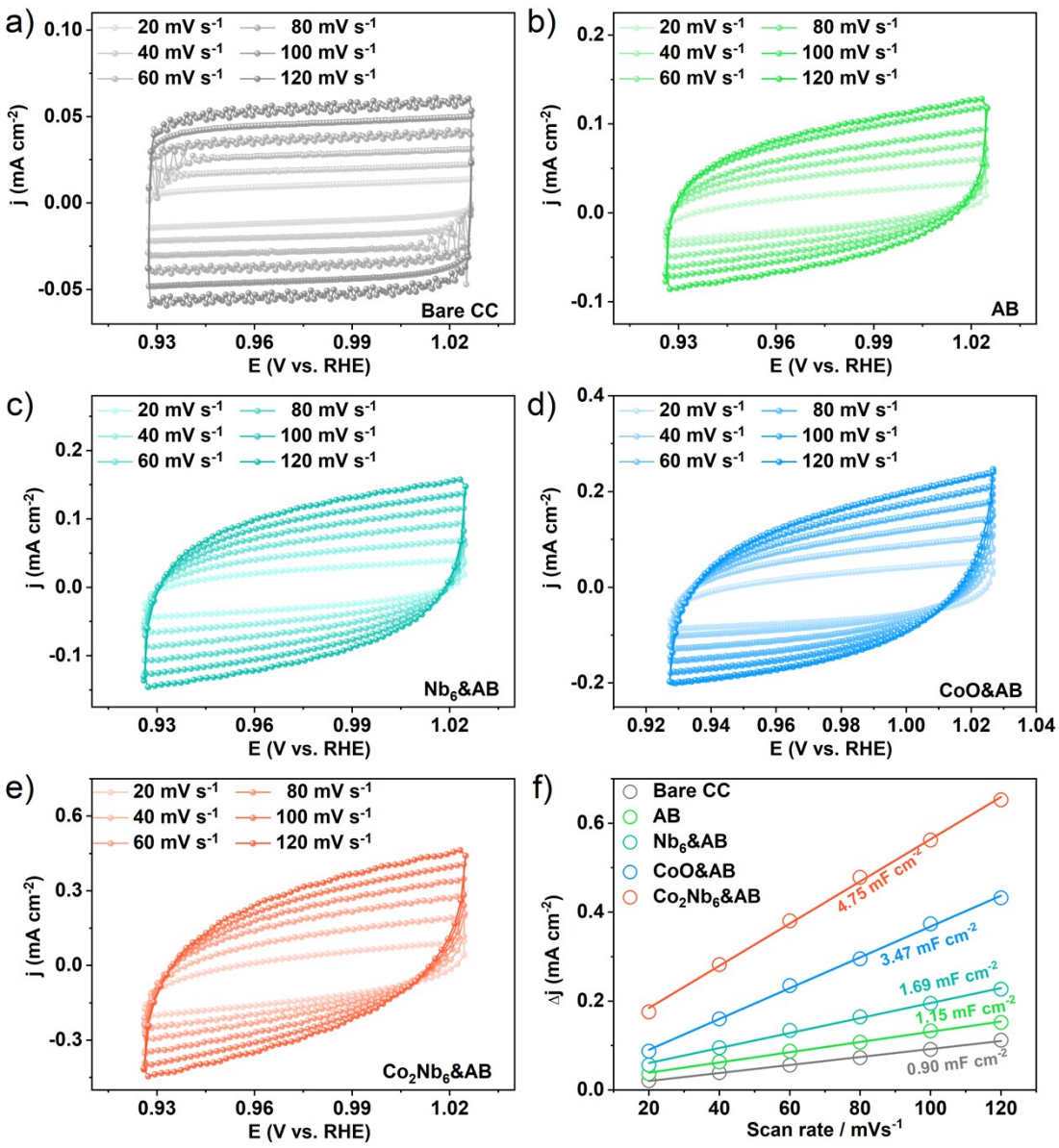

Fig. S6 CV curves for UOR in 1.0 M KOH solution with 0.33 M urea at a scan rate of 20, 40, 60, 80, 100, and 120 and mV s^{-1}: a) Bare CC, b) AB, c) **Nb_6&AB**, d) CoO&AB, e) **Co_2Nb_6&AB**; f) ECSA of each sample, respectively.

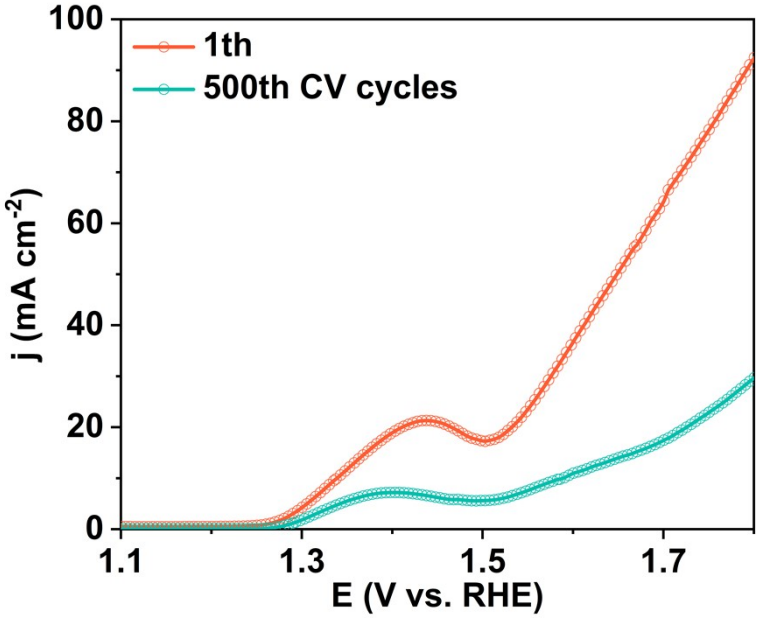

Fig. S7 LSV curves of **Co_2Nb_6/AB** before and after 500 cycles of CV test.

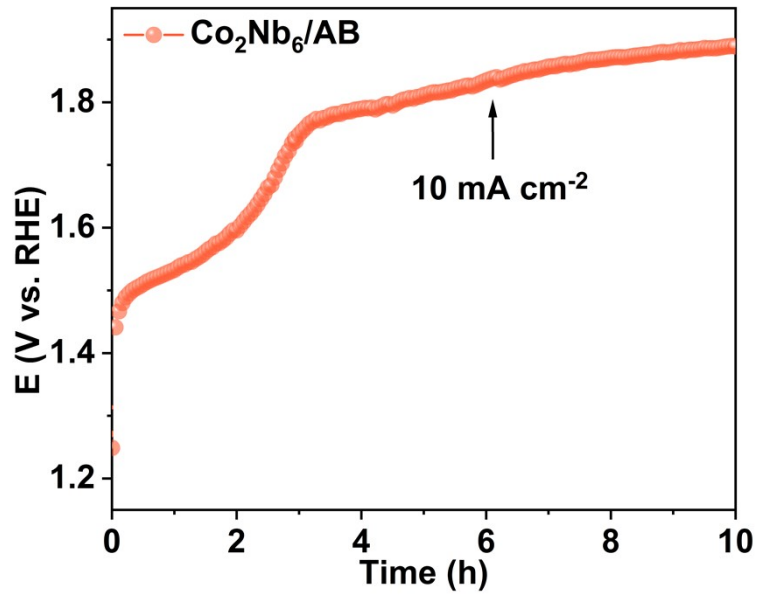

Fig. S8 Chronopotentiometry curve at 10 mA cm^{-2} of the **Co_2Nb_6/AB** anode towards urea electrolysis.

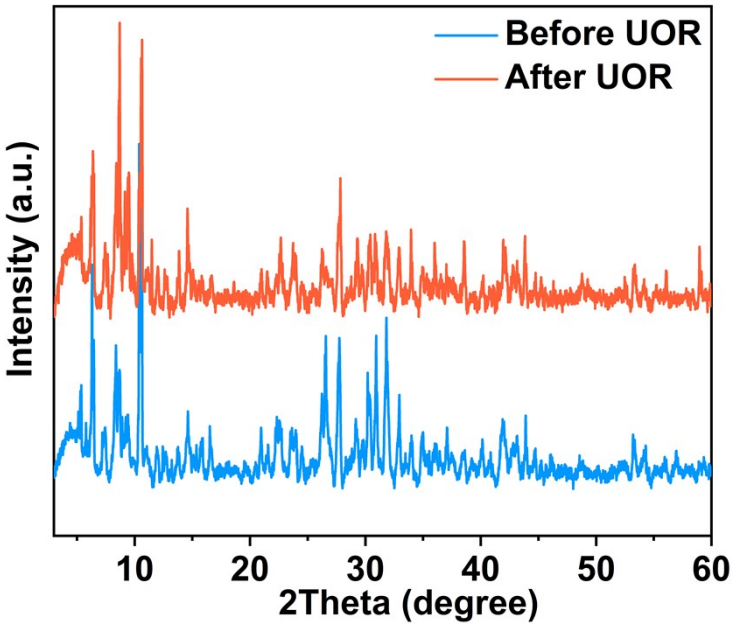

Fig. S9 Powder XRD patterns of **Co_2Nb_6&AB** before and after 10 h UOR.

Notes and references

1. J. Dopta, L. K. Mahnke and W. Bensch, New pronounced progress in the synthesis of group 5 polyoxometalates, *CrystEngComm*, 2020, **22**, 3254–3268.
2. H. Roh, C. Lim, D. Kim, T. Park and K. Yong, Hierarchically nanostructured Ni(Mo,Co)-WO_x electrocatalysts for highly efficient urea electrolysis, *Appl. Surf. Sci.*, 2023, **610**, 155520.
3. Z. Ji, Y. Song, S. Zhao, Y. Li, J. Liu and W. Hu, Pathway manipulation via Ni, Co, and V ternary synergism to realize high efficiency for urea electrocatalytic oxidation, *ACS Catal.*, 2021, **12**, 569–579.
4. J. Shen, Q. Li, W. Zhang, Z. Cai, L. Cui, X. Liu and J. Liu, Spherical Co_3S_4 grown directly on Ni–Fe sulfides as a porous nanoplate array on $FeNi_3$ foam: a highly efficient and durable bifunctional catalyst for overall water splitting, *J. Mater. Chem. A*, 2022, **10**, 5442–5451.
5. S. Zheng, H. Qin, X. Cao, T. Wang, W. Lu and L. Jiao, Electron modulation of cobalt carbonate hydroxide by Mo doping for urea-assisted hydrogen production, *J. Energy Chem.*, 2022, **70**, 258–265.
6. R. Tong, M. Xu, H. Huang, J. Wu, Y. Xiong, M. Shao, Y. Zhao, S. Wang and H. Pan, Co_3Mo_3N nanosheets arrays on nickel foam as highly efficient bifunctional electrocatalysts for overall urea electrolysis, *Int. J. Hydrogen Energy*, 2022, **47**, 11447–11455.
7. N. Shilpa, A. Pandikassala, P. Krishnaraj, P. S. Walko, R. N. Devi and S. Kurungot, Co–Ni layered double hydroxide for the electrocatalytic oxidation of organic molecules: an approach to lowering the overall cell voltage for the water splitting process, *ACS Appl. Mater. Interfaces*, 2022, **14**, 16222–16232.
8. W. Shi, X. Sun, R. Ding, D. Ying, Y. Huang, Y. Huang, C. Tan, Z. Jia and E. Liu, Trimetallic NiCoMo/graphene multifunctional electrocatalysts with moderate structural/electronic effects for highly efficient alkaline urea oxidation reaction, *Chem. Commun.*, 2020, **56**, 6503–6506.
9. W. Huang, Y. Yuan, K. Wang, Q. Cao, Y. Zhao, X. Sun, R. Ding, P. Gao, W. Cai and E. Liu, Tuning interface density and electronic structure of NiS/Ni_3S_4 by Mo, Co co-doping for efficient urea electrooxidation reaction, *J. Electroanal. Chem.*, 2022, **911**, 116242.
10. L. Sha, J. Yin, K. Ye, G. Wang, K. Zhu, K. Cheng, J. Yan, G. Wang and D. Cao, The construction of self-supported thorny leaf-like nickel-cobalt bimetal phosphides as efficient bifunctional electrocatalysts for urea electrolysis, *J. Mater. Chem. A*, 2019, **7**, 9078–9085.

11. C. B. Sun, M. W. Guo, S. S. Siwal and Q. B. Zhang, Efficient hydrogen production via urea electrolysis with cobalt doped nickel hydroxide-riched hybrid films: Cobalt doping effect and mechanism aspect, *J. Catal.*, 2020, **381**, 454–461.
12. Y. Sun, S. Wang, J. Ning, Z. Zhang, Y. Zhong and Y. Hu, A one-pot "shielding-to-etching" strategy to synthesize amorphous MoS_2 modified $CoS/Co_{0.85}$ Se heterostructured nanotube arrays for boosted energy-saving H_2 generation, *Nanoscale*, 2020, **12**, 991−1001.
13. S. Wang, X. Yang, Z. Liu, D. Yang and L. Feng, Efficient nanointerface hybridization in a nickel/cobalt oxide nanorod bundle structure for urea electrolysis, *Nanoscale*, 2020, **12**, 10827−10833.
14. K. Zhang, C. Liu, N. Graham, G. Zhang and W. Yu, Modulation of dual centers on cobalt-molybdenum oxides featuring synergistic effect of intermediate activation and radical mediator for electrocatalytic urea splitting, *Nano Energy*, 2021, **87**, 106217.
15. A. Kumar, X. Liu, J. Lee, B. Debnath, A. R. Jadhav, X. Shao, V. Q. Bui, Y. Hwang, Y. Liu, M. G. Kim and H. Lee, Discovering ultrahigh loading of single-metal-atoms via surface tensile-strain for unprecedented urea electrolysis, *Energy Environ. Sci.*, 2021, **14**, 6494−6505.
16. X. Du, Z. Dai, Y. Wang, X. Han and X. Zhang, Facile synthesis of MWO_4 (M=Co, Ni, Zn and Cu) nanoarrays for efficient urea oxidation, *Int. J. Hydrogen Energy*, 2022, **47**, 8875−8882.
17. C. Zhang, X. Du and X. Zhang, Controlled synthesis of three-dimensional branched Mo–$NiCoP@NiCoP/Ni_XCo_YH_2PO_2$ core/shell nanorod heterostructures for high-performance water and urea electrolysis, *Int. J. Hydrogen Energy*, 2022, **47**, 10825−10836.
18. J. Zhang, S. Huang, P. Ning, P. Xin, Z. Chen, Q. Wang, K. Uvdal and Z. Hu, Nested hollow architectures of nitrogen-doped carbon-decorated Fe, Co, Ni-based phosphides for boosting water and urea electrolysis, *Nano Res.*, 2021, **15**, 1916−1925.
19. W. Zhao, H. Cao, L. Ruan, S. He, Z. Xu and W. Zhang, High-performance self-supporting $AgCoPO_4$/CFP for hydrogen evolution reaction under alkaline conditions, *RSC Adv.*, 2022, **12**, 15751−15758.
20. H. Xu, K. Ye, K. Zhu, J. Yin, J. Yan, G. Wang and D. Cao, Template-directed assembly of urchin-like CoS_x/Co-MOF as an efficient bifunctional electrocatalyst for overall water and urea electrolysis, *Inorg. Chem. Front.*, 2020, **7**, 2602–2610.
21. H. Xu, K. Ye, J. Yin, K. Zhu, J. Yan, G. Wang and D. Cao, In situ growth of ZIF67 at the edge of nanosheet transformed into yolk-shell $CoSe_2$ for high efficiency urea electrolysis, *J. Power Sources*, 2021, **491**, 229592.
22. T. Wang, Y. Cao, H. Wu, C. Feng, Y. Ding and H. Mei, N-doped M/CoO (M=Ni, Co, and Mn) hybrid grown on nickel foam as efficient electrocatalyst for the chemical-assisted water electrolysis, *Int. J. Hydrogen Energy*, 2022, **47**, 5766−5778.
23. W. Yuan, T. Jiang, X. Fang, Y. Fan, S. Qian, Y. Gao, N. Cheng, H. Xue and J. Tian, Interface engineering of S-doped $Co_2P@Ni_2P$ core–shell heterostructures for efficient and energy-saving water splitting, *Chem. Eng. J.*, 2022, **439**, 135743.
24. M. Pan, W. Chen, G. Qian, T. Yu, Z. Wang, L. Luo and S. Yin, Carbon-encapsulated Co_3V decorated Co_2VO_4 nanosheets for enhanced urea oxidation and hydrogen evolution reaction, *Electrochim. Acta*, 2022, **407**, 139882.
25. M. Pan, G. Qian, T. Yu, J. Chen, L. Luo, Y. Zou and S. Yin, Ni modified Co_2VO_4 heterojunction with poor/rich-electron structure for overall urea-rich wastewater oxidation, *Chem. Eng. J.*, 2022, **435**, 134986.